A Physical-Based Algorithm for Retrieving Land Surface Temperature From Moon-Based Earth Observation

Linan Yuan and Jingjuan Liao

***Abstract*—Land surface temperature (LST) is a key parameter and plays an important role in hydrology, ecology, environment, and biogeochemistry. It is difficult for the existing satellites to acquire global LST with spatial and temporal consistency. The Moon-based Earth observation platform with a long life, large coverage can observe continuously the Earth, and obtain the global-scale LST. At present, various approaches for retrieving LST from passive microwave remote sensing data have been developed for the satellite remote sensing data with small and constant viewing zenith angle, however, the Moon-based Earth observation platform located outside the Earth's ionosphere has the viewing zenith angle of 0–90°. In this study, a modified physical-based method of LST retrieval from passive microwave data was developed for wide viewing zenith angles, and the LST and emissivity can be simultaneously estimated through the analysis of various atmospheric and ionosphere parameters. Three types of data, including the FengYun-3B satellite microwave radiation imager data, the multichannel Advanced Microwave Scanning Radiometer data, and Moon-based microwave radiation simulation data with the viewing zenith angles of 52–53°, 55°, and 0–90°, respectively, were used to retrieve LST. Results show that the estimation accuracy of LST decreases with the increase of viewing zenith angle. The 23.8 and 36.5 GHz brightness temperature is optimum for the LST estimation under a large-scale viewing zenith angle, and the root mean square errors of the LST are 5.18, 5.44, and 4.79 K, respectively.**

***Index Terms*—Atmospheric downward radiation, atmospheric transmittance, land surface temperature, LST retrieval, Moon-based Earth observation, the ionosphere.**

I. Introduction

LAND surface temperature is a key parameter in surface heat flux budget and plays an integral role in climate, hydrology, Earth biochemistry, etc. Moreover, it has wide potential applications in agriculture and economy [1], such as crop water requirements assessment, frost damage area evaluation, forest fire detection, and geothermal locations discrimination. With the development of Earth observation technology, the remote sensing technology has become an important tool for rapid estimation of LST. However, the existing satellites cannot acquire Earth observation data on a global scale due to a low orbital altitude and limited field of view [2]. Thus, the acquisition of global land surface temperature with spatial and temporal consistency is difficult through the present algorithm and satellite data. Since the 21st century, the Moon-based Earth observation is gradually paid more attention due to its advantages such as long platform life, large coverage and continuous Earth observation [3]–[5]. The Moon is a natural satellite of the Earth, various sensors placed on it could make comprehensive, continuous, and long-term observations of the Earth. Hence the Moon-based Earth observation platform provide a convenient for estimating the LST at global scale.

The previous studies proposed many methods for estimating LST from passive microwave remote sensing data, which are mainly divided into the statistical-based and physical-based retrieval algorithms. The statistical-based retrieval algorithm is widely used due to the simple arithmetic and easy operation. McFarland *et al.* presented that the scattering and absorption of water vapor, cloud particles and rain have little effect on the low-frequency microwave in the atmosphere [6]. The SSM/I brightness temperature at 37 GHz is optimum for retrieving LST, and the brightness temperature difference between 37 and 19 GHz can be used to correct of the brightness temperature decrease caused by surface water, and water vapor absorption has a large effect on the brightness temperature at 22 and 37 GHz. Holmes *et al.* [7] and Alain *et al.* [8] found that 37 GHz brightness temperature from SMMR and SSM/I can obtain higher estimation accuracy of LST. Based on MODIS LST products, Mao *et al.* analyzed the characteristic of each channels of AMSR-E data, and chose the effective channel to retrieve LST with the multiple linear regression method [9], [10]. The physical-based retrieval algorithm is based on the radiative transfer equation and usually combines some assumptions and simplifications to derive LST. For example, Gao *et al.* developed an algorithm to retrieve LST over the Amazonian forest [11]. The algorithm established the relationships between polarization ratio and surface emissivity for forested and non-forested areas, the LST thus can solely be calculated from microwave radiance. Basist *et al.* developed a LST retrieval algorithm using SSM/I data [12], which adjusted the temperature for variations in surface emissivity. Fily *et al.* found a linear relationship between microwave (19 and 37 GHz) surface emissivity at

Manuscript received December 29, 2019; revised March 30, 2020; accepted April 3, 2020. Date of publication April 16, 2020; date of current version May 18, 2020. This work was supported in part by the National Natural Science Foundation of China under Grant 41590855 and in part by the Key Research Project in Frontier Science of the Chinese Academy of Sciences under Grant QYZDY-SSW-DQC026. *(Corresponding author: Jingjuan Liao.)*

Linan Yuan is with the Aerospace Information Research Institute, Chinese Academy of Sciences, Beijing 100094, China, and also with the University of Chinese Academy of Sciences, Beijing 100049, China (e-mail: yuanln@radi.ac.cn).

Jingjuan Liao is with the Aerospace Information Research Institute, Chinese Academy of Sciences, Beijing 100094, China (e-mail: liaojj@radi.ac.cn).

Digital Object Identifier 10.1109/JSTARS.2020.2987102

horizontal and vertical polarizations over snow and ice-free areas and proposed a LST estimation algorithm neglecting the cosmic space radiation [13]. Weng and Grody proposed a LST retrieval algorithm of two adjacent channels [14]. The algorithm assumed the microwave emissivity of two adjacent frequencies (19.35 GHz and 22.23 GHz) are equal and the brightness temperature difference of two channels is caused by atmospheric effects, then the LST is obtained by Newton iterative processing.

Considering the characteristics of the Moon-based Earth observation platform, several issues must be paid attention when the existing LST retrieval algorithms from microwave remote sensing are directly applied to the Moon-based platform: 1) The statistical-based retrieval algorithm lacks physical significance and the physical-based retrieval algorithm introduces some assumptions or simplifications due to the complex atmospheric radiative transfer, and caused the low inversion precision of LST. 2) The existing LST retrieval algorithms were developed for spaceborne microwave remote sensing data with small and constant zenith angle, while the Moon-based image has the zenith angle of 0–90°. 3) The existing retrieval algorithm neglects the ionosphere due to the low orbital of satellite, while the Moon-based is located outside the Earth' ionosphere and the effect of ionosphere need to be considered. Therefore, a modified physical-based algorithm need be developed to retrieve LST from microwave remote sensing data based on the Moon-based earth observation platform.

II. Data

A. Remote Sensing Data

Three brightness temperature data from the microwave radiation imager (MWRI), the multichannel Advanced Microwave Scanning Radiometer (AMSR-E), and Moon-based microwave radiation simulation were used to retrieve LST and evaluate the accuracy of the physical-based retrieval algorithm.

The MWRI aboard FengYun-3B satellite (FY3B) has five frequencies at 10.65, 18.7, 23.8, 36.5, and 89 GHz, and each frequency has dual channels at vertical and horizontal polarization, respectively. The viewing zenith angle of MWRI data is 52–53°, while its L1 brightness temperature products since October 2013 can be downloaded from the National Satellite Meteorological Center (NSMC) of China Meteorological Administration (CMA). Thus, the MWRI data on January 1–2, 2018 was selected for this study.

The AMSR-E is a conically scanning total power passive microwave radiometer sensing microwave radiation (brightness temperatures) at 12 channels and 6 frequencies ranging from 6.9 to 89.0 GHz. Horizontally and vertically polarized radiation is measured separately at each frequency with the viewing zenith angle of 55°. The AMSR-E daily brightness temperature products with a 0.25° spatial resolution on January 1-9, 2005 is provided by the National Snow and Ice Data Center (NSIDC).

The Moon-based microwave radiation data was obtained by microwave imaging simulation. At present, the research on moon-based Earth observation is still in the stage of theoretical analysis without actual available data. Theoretically, each image acquired at some moment (Coordinated Universal Time: UTC) by a Moon-based platform can cover almost half of the Earth's surface, spanning 12 time zones. The imaging position of the Moon-based Earth observation changes with the relative movement of the Earth and the Moon. Based on the performance analysis of the Moon-based Earth observation platform, several factors affecting the moon-based microwave radiation imaging, including time zone correction, Earth-Moon relative movement, atmospheric radiative transfer and ionospheric effect, were analyzed and a method for simulating the moon-based microwave brightness temperature images was developed. Firstly, the JNG06 land-surface diurnal temperature cycle model was applied to obtain the global surface temperatures at the same coordinated universal time using spaceborne LST and sea surface temperature products. Then the Jet Propulsion Laboratory (JPL) ephemeris data was used to simulate the coverage of Moon-based imaging and the zenith angle distribution. Finally, the Moon-based microwave radiation brightness temperature images was obtained based on the estimation of the atmospheric radiative transfer and analysis of the ionosphere effect. The details of Moon-based microwave radiation simulation can see the reference [15]. The Moon-based microwave radiation simulation data used in this study operates six frequencies, including 6.9, 10.8, 18.7, 23.8, 36.5, and 89.0 GHz, and each frequency have horizontal and vertical polarization modes with the zenith angle of 0–90°. The image time was selected on January 1, 2005.

B. LST In Situ Measurements

U.S. Climate Reference Network (USCRN) is a nationwide network which can provide continuous and high-quality data of ground surface temperature [16]. The network consists of approximately 300 stations across the continental United States, Alaska, and Hawaii. The network provided thermal infrared LST at different time in hours, days, and months since 2002. In this article, the USCRN LST data consistent with the remote sensing data was used as the real surface temperature to verify the LST derived from three kinds of brightness temperature, e.g., the MWRI brightness temperature, the AMSR-E brightness temperature, and Moon-based microwave radiation simulations. Then several parameters such as the average error, the root mean square error (RMSE), and temperature variation range are selected to validate the accuracy of estimation results.

III. Methods

A. The Moon-Based LST Retrieval Algorithm

The basis of LST retrieval from passive microwave data is the surface heat radiation conduction which is described by the microwave radiation transfer equation. It can be found that the total radiation intensity received by the Moon-based microwave radiometer include not only the microwave radiation from the Earth's surface, but also the atmospheric upward and downward radiations. Due to the attenuation caused by the atmosphere and the ionosphere, the radiation energy of microwave reduced during the process of reaching the Moon-based platform. Therefore, the LST estimation from microwave remote sensing data is actually a complicated problem. Based on the atmospheric radiation

transmission theory and microwave propagation in the ionosphere [6]–[14], [17]–[19], the total radiant energy received by a Moon-based microwave radiometer comprises three sections: 1) microwave radiation of the Earth's surface after the attenuation of atmosphere and ionosphere; 2) The atmospheric downward, firstly reflected by the Earth's surface and then attenuated by the atmosphere and ionosphere; 3) The atmospheric upward radiation attenuated by ionosphere. Consequently, the general radiance transfer equation for microwave can be expressed as [20], [21]

$$B_f\left(T_f\right) = \left[\tau_f\left(\theta\right)\varepsilon_p B_f\left(T_s\right) + \tau_f\left(\theta\right)\left(1-\varepsilon_p\right)B_f\left(T_a^{\downarrow}\right) + B_f\left(T_a^{\uparrow}\right)\right]\cdot\varphi\left(f,\theta\right) \tag{1}$$

where T_f is the brightness temperature in frequency of f, $\tau_{\mathrm{f}}(\theta)$ is the atmospheric transmittance at the viewing zenith angle of θ, ε_p is the surface emissivity for the polarization p, $\mathrm{T_S}$ is the LST, T_a is the average atmospheric temperature. $B_f(T_s)$ is the microwave radiation of the Earth's surface, $B_f(T_a^{\downarrow})$ is the downwelling path radiance, $B_f(T_a^{\uparrow})$ is the upwelling path radiance, and $\varphi(\mathrm{f},\theta)$ is the attenuation of microwave energy in the ionosphere. $B_f(T)$ is the Planck function, which describes the relationship between the emissivity of electromagnetic radiation emitted from a blackbody and the frequency of electromagnetic radiation of any temperature. The Planck function is given by

$$B_f\left(T_i\right) = \frac{2hf^3}{c\left(e^{hf/kT}-1\right)} \tag{2}$$

where $B_f(T_i)$ is the blackbody spectral brightness with the unit of $\mathrm{W}\cdot m^{-2}\cdot sr^{-1}\cdot Hz^{-1}$, h is the Planck constant with the value of $6.63\times10^{-34}J$, f is the frequency, k is the Boltzmann constant with the value of $1.38\times10^{-23}J\cdot K^{-1}$, c is velocity of light with the value of 2.992×10^{8} ms^{-1}, T is the absolute temperature in Kelvin. Based on the Rayleigh-Jeans approximation in the microwave band, (2) can be simplified as

$$B_f\left(T_i\right) = \frac{2kT}{\lambda^2} \tag{3}$$

Therefore, (1) can be expressed as

$$T_{B,P} = \left[\tau_f\left(\theta\right)\cdot\varepsilon_p\cdot T_S + \tau_f\left(\theta\right)\cdot\left(1-\varepsilon_p\right)\cdot T_{atm\downarrow} + T_{atm\uparrow}\right]\cdot\varphi\left(f,\theta\right) \tag{4}$$

where $\mathrm{T_{B,P}}$ is the brightness temperature, $\tau_f(\theta)$ is the atmospheric transmittance, and ε_{p} is the surface emissivity for the polarization p, $\mathrm{T_{atm\uparrow}}$ is the atmospheric upward radiation, $\mathrm{T_{atm\downarrow}}$ is the atmospheric downward radiation, $\varphi(f,\theta)$ is the attenuation of microwave energy in the ionosphere.

From the moon-based radiation transfer equation of single channel, there are at least two unknown parameters, such as the LST and the surface emissivity, and the effect of atmosphere and ionosphere need to be resolved. In addition, another parameter will increase even if one more channel is added. The theoretical expression of Moon-based brightness temperature in horizontal and vertical polarization ($\mathrm{T_{B,h}}/\mathrm{T_{B,v}}$) can be obtain with three unknown parameters, such as LST and horizontal and vertical microwave surface emissivity. Since the number of unknown parameters is more than the number of equations, it is necessary to resolve the microwave surface emissivity in order to estimate the LST. Royer and Poirier found an empirical linear relationship between the surface emissivity of horizontal and vertical polarization [8]

$$\varepsilon_v = a * \varepsilon_h + b \tag{5}$$

where $\varepsilon_{\mathrm{v/h}}$ is the surface emissivity of vertical and horizontal polarization, a and b are the coefficients and offsets of the relationship between the vertical and horizontal emissivity. They are derived by the radiation transfer equation at large-scale Moon-based Earth observation, which is expressed as (6).

$$\varepsilon_{\mathrm{p}} = \frac{T_{\mathrm{BT}} - T_{\mathrm{atm\_up}} - T_{\mathrm{atm\_down}}\cdot\gamma}{\gamma\cdot\left(T_0 - T_{\mathrm{atm\_down}}\right)} \tag{6}$$

where T_{BT} is brightness temperature, T_0 is LST, $T_{\mathrm{atm\_up}}$ is atmospheric downward radiation, $T_{\mathrm{atm\_up}}$ is atmospheric upward radiation, γ is atmospheric transmittance.

In this study, the microwave brightness temperature data, thermal infrared temperature data and atmospheric profile data from satellites were used to evaluate the value of horizontal and vertical microwave emissivity at 6.9, 10.8, 18.7, 23.8, 36.5, and 89.0 GHz [22]. Then a regression analysis between horizontal and vertical microwave emissivity was developed to obtain the correlation coefficient R^2 and the expression, as shown in Fig. 1. The coefficients and offsets (a and b) can be obtained from the expression, such as the coefficients for 6.9, 10.8, 18.7, 23.8, 36.5, and 89.0 GHz is 0.505, 0.551, 0.608, 0.639, 0.716, and 0.869, and the offsets is 0.504, 0.455, 0.393, 0.366, 0.287, and 0.143, respectively. In addition, the correlation coefficient R^2 at

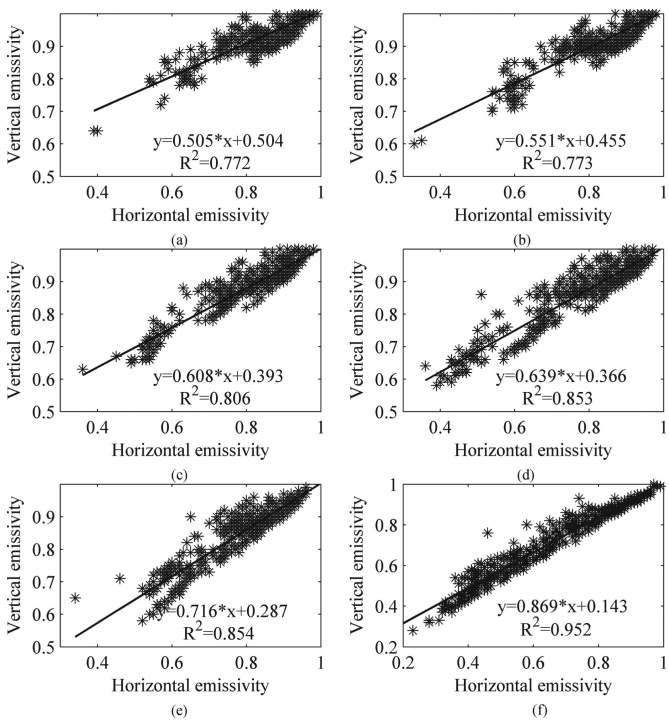

Fig. 1. The relationship between the horizontal and vertical microwave emissivity at different frequency. (a) 6.9 GHz. (b) 10.8 GHz. (c) 18.7 GHz. (d) 23.8 GHz. (e) 36.5 GHz. (f) 89.0 GHz.

6.9, 10.8, 18.7, 23.8, 36.5, and 89.0 GHz is 0.772, 0.773, 0.806, 0.853, 0.854, and 0.952. Results show that the linear correlation coefficient between horizontal and vertical microwave emissivity for different frequencies are between 0.77 and 1.0, so that the significant linear correlation of the surface emissivity can be used for LST estimation.

Using on the relationship between the horizontal and vertical microwave emissivity and the theoretical model of Moon-based microwave radiation brightness temperature, the LST and horizontal as well as vertical microwave emissivity can be simultaneously obtained through the analysis of atmospheric transmittance, atmospheric upward and downward radiations, and the attenuation of microwave energy in the ionosphere and viewing zenith angle. The LST and microwave emissivity can be expressed as (7)–(9) shown at the bottom of this page.

Based on the brightness temperature of each microwave frequency at vertical and horizontal polarization, the LST can be estimated. In this study, five frequencies from FY3B MWRI, six frequencies from AMSR-E, and six frequencies from Moon-based microwave radiation simulations are used to estimate the LST, respectively.

B. The Parameters Estimation

In order to retrieve the LST using the Moon-based LST retrieval algorithm, we need to estimate these parameters, including microwave atmospheric transmittance, atmospheric upward and downward radiations, and the attenuation of microwave energy caused by ionosphere.

1) The Atmospheric Attenuation of Microwave: The atmospheric attenuation of microwave is mainly related to the absorption and scattering of oxygen and water vapor. Since the molecules of oxygen and water vapor in the atmosphere are much smaller than microwaves, the scattering from the molecules of oxygen and water vapor can be ignored. Thus, the atmospheric attenuation of microwave is mainly caused by the absorption from the molecules of oxygen and water vapor [23], [24]. In this study, we applied the method in the International Telecommunication Union Radio communication sector (ITU-R) P Series P.676-8 recommendation [25] to calculate the atmospheric attenuation by accumulating the respective resonant lines of oxygen and water vapor. The atmospheric attenuation of microwave is given by

$$\gamma = \gamma_o + \gamma_w = 0.1820 f N''(f) \tag{10}$$

where γ_o and γ_w is the atmospheric attenuation of microwave under dry air (oxygen, pressure-induced nitrogen and non-resonant Debye attenuation) and water vapor conditions, f is the frequency, $N''(f)$ is the imaginary part of the frequency-dependent complex refractivity

$$N''(f) = \sum_i S_i F_i + N''_D(f) \tag{11}$$

where S_i is strength of the i-th line, F_i is the line shape factor and the sum extends over all the lines (for the frequencies above 118.75 GHz, only the oxygen lines above 60 GHz should be included in the summation) and $N''_D(f)$ is the dry continuum due to pressure-induced nitrogen absorption and the Debye spectrum. The S_i for oxygen and water vapor can be expressed as (12) and (13)

$$S_{io} = a_1 \times 10^{-7} \cdot p \cdot \theta^3 \cdot \exp\left[a_2 \cdot (1-\theta)\right] \tag{12}$$

$$S_{iw} = b_1 \times 10^{-1} \cdot e \cdot \theta^{3.5} \cdot \exp\left[b_2 \cdot (1-\theta)\right] \tag{13}$$

where p is dry air pressure, e is the water vapor partial pressure, θ is 300/T and T is the temperature (in K). a_1 and a_2 is the attenuation coefficients in oxygen, b_1 and b_2 is the attenuation coefficients in water vapor.

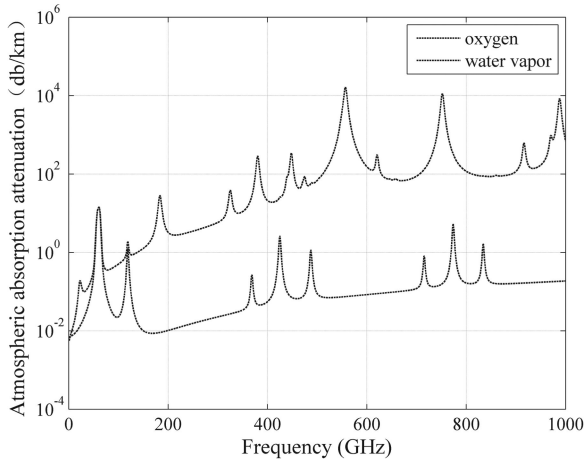

Fig. 2. Microwave atmospheric attenuation contributed from the oxygen and the water vapor.

Fig. 2 shows the atmospheric attenuation from the oxygen and the water vapor with the frequency of 0–1000 GHz, and multiple water vapor and eight oxygen absorption peaks and are presented from 0 to 1000 GHz.

2) Atmospheric Transmittance, Upward and Downward Radiations: The atmospheric transmittance is the ratio of the electromagnetic radiation flux after atmospheric attenuation to the

$$T_S = \frac{T_{B,V} - a \cdot T_{B,H} - \left[\tau_f(\theta) \cdot (1-a-b) \cdot T_{\mathrm{atm}\downarrow} + (1-a) \cdot T_{\mathrm{atm}\uparrow}\right] \cdot \varphi(f,\theta)}{\tau_f(\theta) \cdot b \cdot \varphi(f,\theta)} \tag{7}$$

$$\varepsilon_h = \frac{b \cdot \left[T_{B,h} - \left(\tau_f(\theta) \cdot T_{\mathrm{atm}\downarrow} + T_{\mathrm{atm}\uparrow}\right) \cdot \varphi(f,\theta)\right]}{T_{B,V} - a \cdot T_{B,H} - \left[\tau_{f(\theta)}(1-a-b) \cdot T_{\mathrm{atm}\downarrow} + (1-a) \cdot T_{\mathrm{atm}\uparrow}\right] \cdot \varphi(f,\theta)} \tag{8}$$

$$\varepsilon_h = \frac{b \cdot \left[T_{B,h} - \left(\tau_f(\theta) \cdot T_{\mathrm{atm}\downarrow} + T_{\mathrm{atm}\uparrow}\right) \cdot \varphi(f,\theta)\right]}{T_{B,V} - a \cdot T_{B,H} - \left[\tau_f(\theta)(1-a-b) \cdot T_{\mathrm{atm}\downarrow} + (1-a) \cdot T_{\mathrm{atm}\uparrow}\right] \cdot \varphi(f,\theta)} \tag{9}$$

incident electromagnetic radiation flux. It is an important factor affecting the microwave radiative transfer. The atmospheric transmittance over a certain area is greatly affected by weather conditions. In a short time, the variation of meteorological parameters, e.g., the atmospheric pressure, humidity, and gas density, lead to a large change of the transmittance [26]–[32]. In microwave bands, its theoretical formula can be expressed as

$$\tau_f(\theta) = \exp\left(-\int_0^{\infty} k_e(z) \cdot \sec\theta \, dz \right. \tag{14}$$

where z is the height, $\mathrm{k_e(z)}$ is atmospheric attenuation coefficient, and θ is the viewing zenith angle.

From (14), the atmospheric transmittance depends on the atmospheric attenuation and the viewing zenith angle. Each image from the Moon-based Earth observation with the zenith angle of 0–90° has variable value of the atmospheric transmittance within the coverage of Moon-based imaging, but the atmospheric transmittance of satellite image is considered a constant. Therefore, the variable atmospheric transmittance can influence the accuracy of the physical-based retrieval algorithm for land surface temperature from Moon-based Earth observation.

The theoretical formula for the radiative transfer equation of atmospheric upward and downward radiations without rainfall can be expressed as [33]–[42]

$$T_{\mathrm{atm}\downarrow} = \int_0^{\infty} T(z) \cdot k_e(z) \cdot \sec\theta \cdot \exp\left(-\int_0^{z} k_e(z') \cdot \sec\theta dz'\right) dz \tag{15}$$

$$T_{\mathrm{atm}\uparrow} = \int_0^{\infty} T(z) \cdot k_e(z) \cdot \sec\theta \cdot \exp\left(-\int_z^{\infty} k_e(z') \cdot \sec\theta \, dz'\right) dz. \tag{16}$$

with,

$$\tau(0,z) = \exp\left(-\int_0^{z} k_e(z') \cdot \sec\theta \, dz'\right) \tag{17}$$

$$\tau(z,\infty) = \exp\left(-\int_z^{\infty} k_e(z') \cdot \sec\theta \, dz'\right) \tag{18}$$

where $T(z)$ is the air temperature, $k_{\mathrm{e}}(z)$ is the atmospheric attenuation, $\tau(s,s')$ the atmospheric optical thickness, and θ is the zenith angle.

The atmospheric upward and downward radiations are related to atmospheric temperature, attenuation, and optical thickness, and will affect the performance of the physical-based retrieval algorithm. The atmospheric temperature is related to the altitude. When the elevation is below 10 km, the atmospheric temperature decreases by about 6.5 °C as the altitude increases by 1 km. Furthermore, the atmospheric temperature remains stable when the elevation is between 10 and 20 km. The atmospheric attenuation depends on the concentration of oxygen and water vapor, and changes with the altitude.

3) Ionospheric Attenuation Effect: The ionosphere extends from about 90 km above the ground to the upper atmosphere of the Earth at an altitude of 1000 km. There are quite a lot of free electrons and ions in the ionosphere, which can change the propagation speed of microwave and cause refraction, reflection, and scattering. These electrons and ions will also cause the attenuation of incident microwave radiation energy due to their collisions in the ionosphere [43]–[48]. Due to the complex nature of the ionosphere, the microwave energy has different attenuation effects at different altitudes of the ionosphere with the change of electron concentration. The attenuation coefficient α at any altitude can be expressed as

$$\alpha = \frac{\omega}{\sqrt{2}c} \cdot \left(\sqrt{\left(1 - \frac{\omega_p^2}{\omega^2 + v_m^2}\right)^2 + \left(\frac{v_m}{\omega} \cdot \frac{\omega_p^2}{\omega^2 + v_m^2}\right)^2} - \left(1 - \frac{\omega_p^2}{\omega^2 + v_m^2}\right)\right)^{1/2} \tag{19}$$

with,

$$\omega_p = e\left(m\varepsilon_0\right)^{-1/2} N_e^{1/2} \tag{20}$$

where ω is the angular frequency of microwave, v_m is the electron collision frequency, ω_p is the plasma frequency, e is the elementary charge, m is the electron mass, ε_0 is the permittivity of vacuum, N_e is the electron concentration. It is described by an empirical model for the vertical distribution of the electron concentration in the ionosphere.

The total attenuation of microwave energy in the ionosphere can be obtained by integrating the attenuation coefficient α along the propagation path of the microwave in the ionosphere. The total attenuation can be expressed as

$$\mathrm{Att}(db) = 8.68 \int_s \alpha \, ds \tag{21}$$

where s is the propagation path of microwave in the ionosphere.

IV. Results and Discussion

A. Results of the Parameters Estimation

Since about 75% air and more than 90% water vapor exists in the range of 10 km above the Earth surface, the atmospheric absorption attenuation is gradually decreasing until it is close to zero with the increase of height [49]. In this study, the atmosphere within 20 km above the Earth's surface is divided into 40 layers in the vertical direction, with 0.5 km per layer. Based on this, the atmospheric attenuation and optical thickness of each layer can be calculated. Then the microwave atmospheric transmittance, atmospheric upward and downward radiations for Moon-based Earth observation can be obtained based on the theoretical expression.

Fig. 3 shows the change of the atmospheric transmittance for Moon-based Earth observation. From this figure, the atmospheric transmittance is related to the atmospheric humidity, the air temperature, the viewing zenith angle, and the frequency. With the increase of the atmospheric humidity, the atmospheric transmittance gradually increases up to 1 [Fig. 3(a)]. When the atmospheric humidity is zero, the atmospheric transmittances of six frequencies, i.e., 6.9, 10.8, 18.7, 23.8, 36.5, and 89.0 GHz, are different and the smallest is about 0.74 at 89.0 GHz. As the

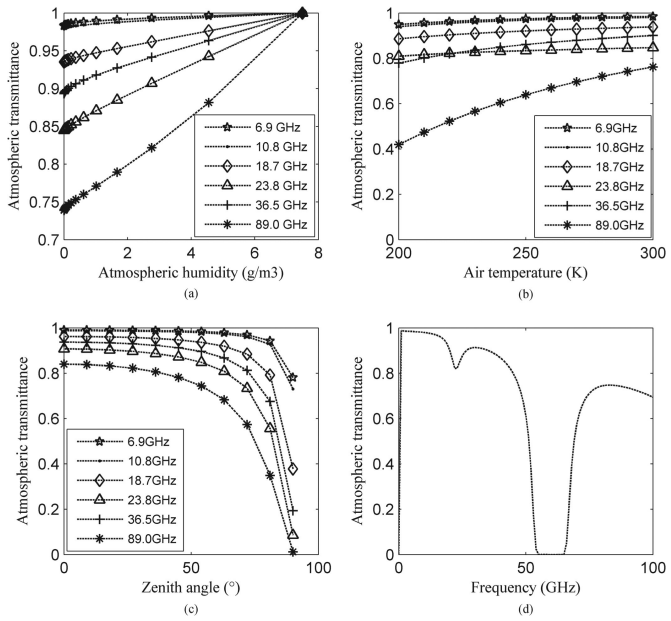

Fig. 3. The change of atmospheric transmittance for Moon-based Earth observation with four factors. (a) The atmospheric humidity. (b) The air temperature. (c) The viewing zenith angle. (d) The frequency.

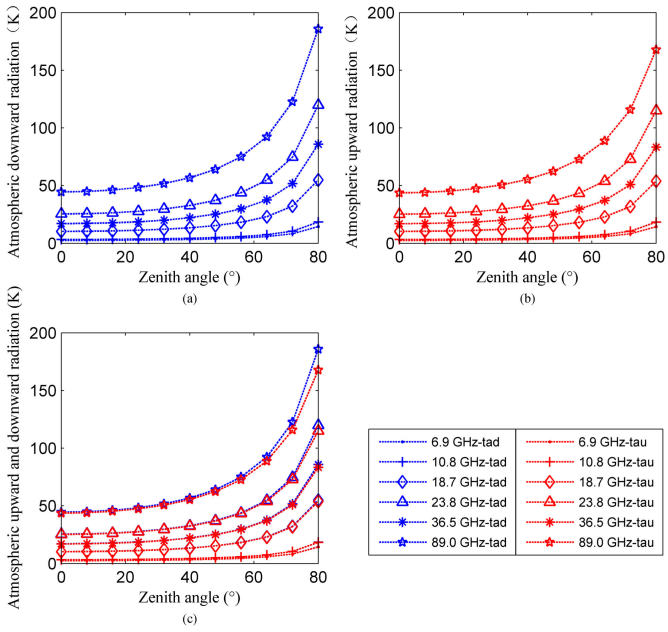

Fig. 4. The atmospheric upward and downward radiations for the Moon-based Earth observation. (a) The atmospheric downward radiation. (b) The atmospheric upward radiation. (c) The comparison of the atmospheric upward and downward radiations for the Moon-based Earth observation. "tad" and "tau" represent the atmospheric downward and upward radiations.

air temperature increases from 200 K to 300 K, the atmospheric transmittance grows slowly except that the 89.0 GHz has a higher grow rate [Fig. 3(b)]. Since there is a strong atmospheric attenuation at 89.0 GHz, mainly the absorption of water vapor, and the air temperature is an essential parameter in the calculation of atmospheric attenuation. Hence the change of air temperature has a large effect on the 89.0 GHz, and the radiation energy received by the Moon-based microwave radiometer decreased rapidly with the increase of air temperature. There is a negative correlation between the atmospheric transmittance and the viewing zenith angle, and the atmospheric transmittance decreases gradually with the increasing zenith angle [Fig. 3(c)]. When the zenith angle is less than 50°, the atmospheric transmittance changes slowly, and the atmospheric transmittance for 6.9, 10.8, 18.7, 23.8, 36.5, and 89.0 GHz are about 0.98, 0.98, 0.95, 0.90, 0.92, and 0.80, respectively. When the zenith angle is greater than 50°, the atmospheric transmittance is greatly affected by the zenith angle, and decreases rapidly with the increase of the zenith angle. There is a nonlinear relationship between frequency and atmospheric transmittance [Fig. 3(d)]. When the frequency is between 0 and 50 GHz, as well as 70 to 100 GHz, it has a bigger atmospheric transmittance than other frequencies, indicating that these frequencies are suitable for Earth observation. While the atmospheric transmittance decreases rapidly up to 0, then increase with the frequency of 50–70 GHz.

Based on (15)–(18), the atmospheric upward and downward radiations for the Moon-based Earth observation can be obtained (Fig. 4). Results show that the atmospheric upward and downward radiations have an obviously positive correlation with the viewing zenith angle. When the viewing zenith angle is less than 40°, the atmospheric radiations vary slowly. When the viewing zenith angle is greater than 40°, it has a significant

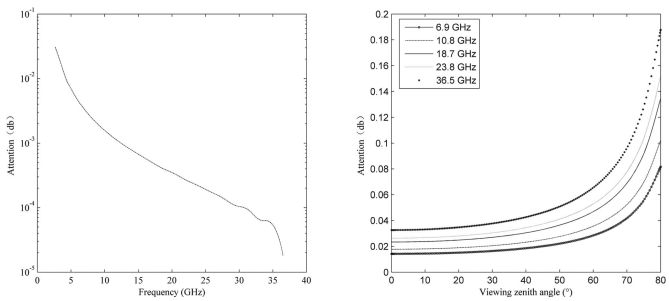

Fig. 5. The energy attenuation in the ionosphere with frequency and the viewing zenith angle. (a) The frequency. (b) The viewing zenith angle.

effect on the atmospheric radiations. Moreover, the atmospheric upward and downward radiations are both related with the microwave frequency. From the figure, the atmospheric downward radiation is slightly larger than the atmospheric upward radiation, but the difference of the two radiations increases with the increase of microwave frequency and the viewing zenith angle.

The attenuation of microwave energy in the ionosphere depends on the microwave frequency and the viewing zenith angle (Fig. 5). As the frequency increases from 0 GHz to 40 GHz, the effect of the ionosphere on microwave transmission gradually decreases [Fig. 5(a)]. The frequency change of less than 25 GHz has a great effect on the attenuation of microwave energy. When the frequency is greater than 25 GHz, the attenuation of the microwave energy in the ionosphere slowly decreases with the increase of frequency. In addition, the viewing zenith angle is a significant factor of the energy attenuation of microwave

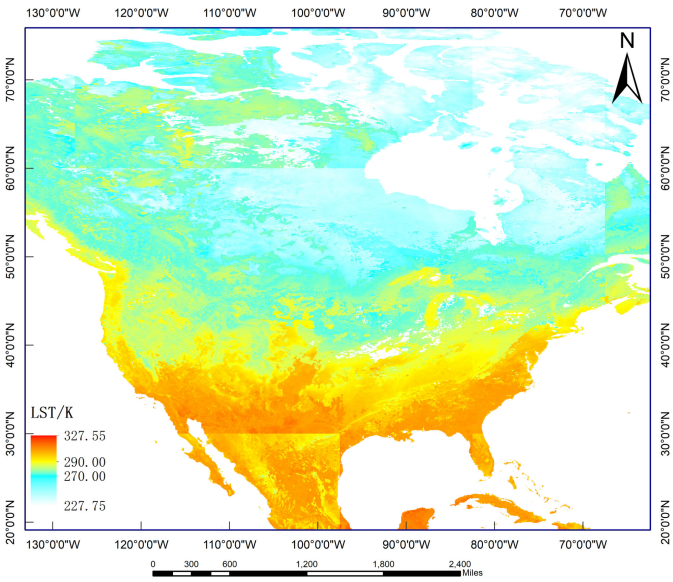

Fig. 6. The LST estimation based on Moon-based microwave radiation simulated data on January 1, 2005.

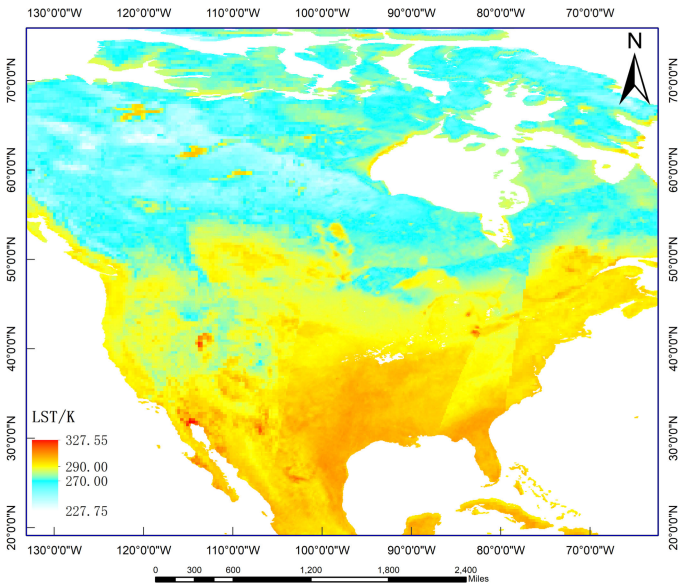

Fig. 7. The LST estimation based on AMSR-E data on January 9, 2005.

propagation in the ionosphere [Fig. 5(b)]. The attenuation of microwave energy increases with the increase of the propagation path of microwave in the ionosphere, which has positive correlation with the zenith angle. Thus, the microwave at large viewing zenith angle has stronger energy attenuation than the small zenith angle. Above all, the attenuation of microwave energy in the ionosphere depends on the viewing zenith angle and the frequency, and increases with the increasing viewing zenith angle and the decreasing frequency.

B. The LST Estimation

Based on the parameter analysis of the Moon-based LST retrieval algorithm from the passive microwave data, the Moon-based microwave radiation simulation data, AMSR-E data, and FY-3B MWRI data with the zenith angle of 0–90°, 55°, and 52–53°, respectively, were used to estimate LST (Figs. 6–8). In the inversion process, the parameters can be simplified for AMSR-E data, and FY-3B MWRI data due to its small and constant viewing zenith angle.

Fig. 6 shows the LST estimation results of Moon-based microwave radiation simulated data on January 1, 2005. From the figure, it can be seen that the temperature in Mexico is higher than in Canada and the United States, about 270–290 K. This is because that the east, west, and south are surrounded by the Madre Mountains and the central part is the Mexican Plateau, causing higher temperature in Mexican than the plain. In the United States, the southern and eastern regions have significantly higher temperature than the north region. The eastern Canada region has slightly lower temperature compared with the central and southern regions. Fig. 7 shows the LST estimation based on AMSR-E data on January 9, 2005. Compared with the estimation of the Moon-based microwave LST on January 1, 2005, the temperature in the central and northern regions of the United States has a slight increase. It is caused by local weather

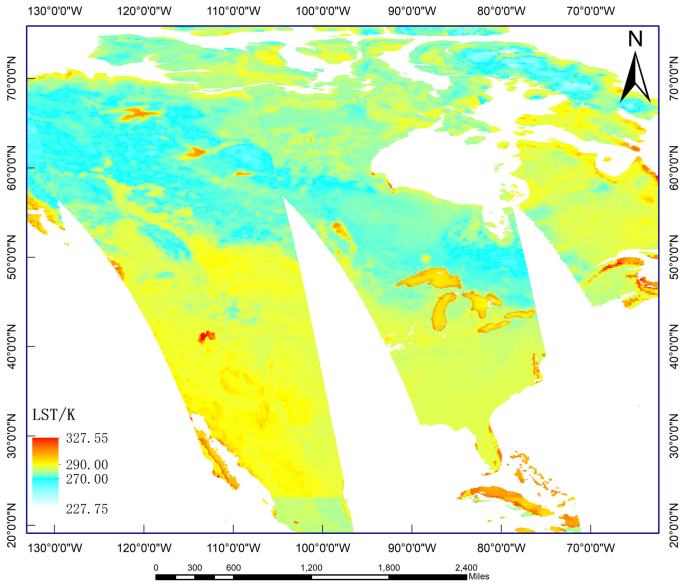

Fig. 8. The LST estimation based on FY-3B MWRI data on January 1, 2018.

changes and temperature inversion errors. Fig. 8 shows the LST estimation of the FY-3B MWRI data on January 1, 2018. It can be seen that the LST in northeastern Canada region has increased a lot relative to 2005 (Figs. 6–8), and the LST in the southern coastal areas of Mexico has partially decreased. The phenomenon is related to local climate change. From Fig. 8, the lake areas, such as Lake Superior, Lake Michigan, Lake Huron, Lake Erie, and Lake Ontario, have large retrieval errors. The reason is that the Moon-based LST retrieval algorithm was developed for land surface, and all parameters of this algorithm, including microwave atmospheric transmittance, atmospheric upward and downward radiations, the attenuation of microwave energy caused by ionosphere, the coefficients and offsets of

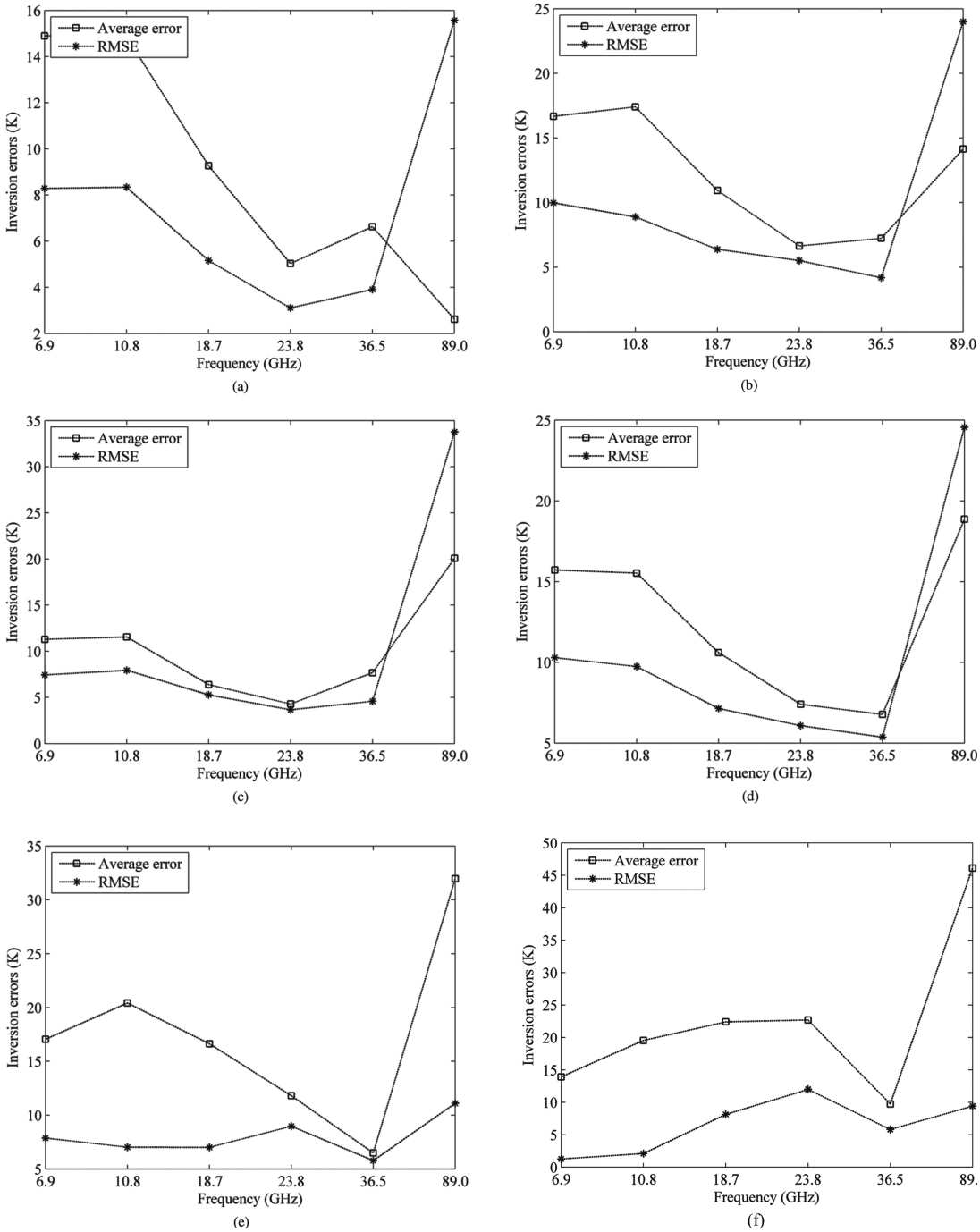

Fig. 9. Accuracy analysis of LST estimation from Moon-based earth observation at: (a) the zenith angle of 0–30°; (b) the zenith angle of 30–40°; (c) the zenith angle of 40–50°; (d) the zenith angle of 50–60°; (e) the zenith angle of 60–70°; (f) the zenith angle of 70–90°.

the relationship between the vertical and horizontal emissivity, were estimated based on the land surface features. However, the radiation characteristics have different performances in land and water surfaces, so the LST estimates using the Moon-based LST retrieval algorithm have higher accuracy than the water surface temperature estimates, indicating that the retrieval algorithm is not suitable for estimating the temperature from water surface.

C. Evaluation of LST Estimation Results

In this study, the measured LST data from the USCRN consistent with the inversion result are used to evaluate the LST derived from FY-3B MWRI, AMSR-E brightness temperature data, and the simulated Moon-based microwave radiation brightness temperature data, respectively. Then the evaluation indicators such as the average error, the RMSE, and the diurnal

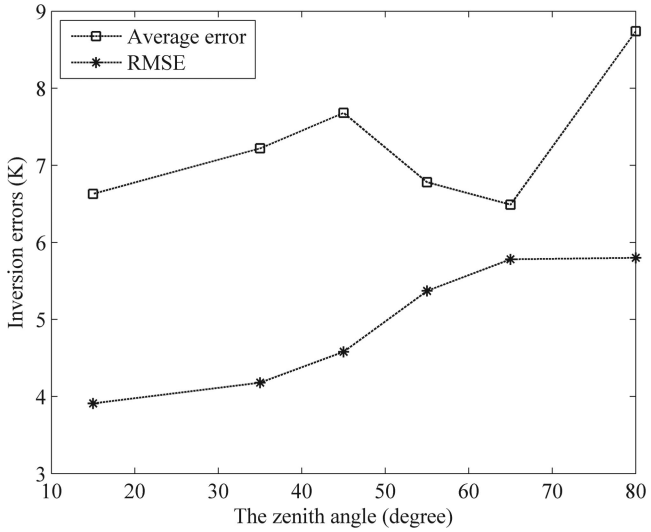

Fig. 10. The change of LST estimation errors with the zenith angle.

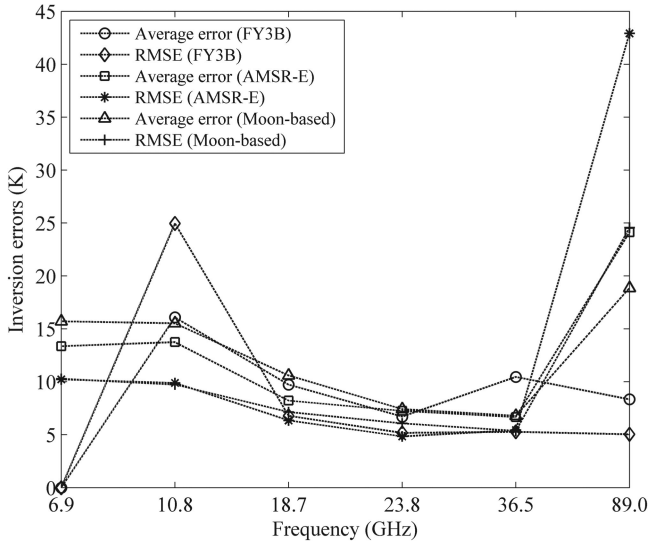

Fig. 11. The LST estimation error from Moon-based microwave radiation brightness temperature data, FY3B MWRI brightness temperature data and AMSR-E data with the same viewing zenith angle.

TABLE I
THE LST ESTIMATION ERROR FROM FY3B MWRI, AMSR-E AND MOON-BASED MICROWAVE RADIATION SIMULATION DATA

Data	Average error/K	RMSE/K	Temperature range/
FY3B MWRI	6.71	5.18	-27.9 ~ 32.4
AMSR-E	6.67	5.44	-28.9 ~ 32.0
Moon-based simulation data	7.09	4.79	-26.0 ~ 32.0

temperature variation are selected to analyze the accuracy of the LST inversion (Figs. 9–11 and Table I).

Fig. 9 is the LST estimation error using the 6.9, 10.8, 18.7, 23.8, 36.5, and 89 GHz microwave brightness temperature data at different viewing zenith angles. When the viewing zenith angle is 0–30° and 40–50°, the LST retrieved from 23.8 GHz brightness temperature data has the lowest average error and RMSE than other LST estimation. Thus the 23.8 GHz is optimum frequency for retrieving LST with the viewing zenith angle of 0–30° and 40–50°. When the viewing zenith angle is 30–40° and 50–90°, the LST retrieved from 36.5 GHz brightness temperature data has the lowest average error and RMSE than other LST estimation. Thus the 36.5 GHz is optimum frequency for retrieving LST with the viewing zenith angle of 30–40° and 50–90°. Overall, the LST derived from 23.8 and 36.5 GHz brightness temperature data have higher accuracy than that of 6.9, 10.8, 18.7, and 89 GHz brightness temperature data, and the two frequencies are more suitable for the LST retrieval at Moon-based large-scale zenith angle.

Fig. 10 shows the change of LST estimation errors with the zenith angle. With the increase of the zenith angle, the average error of LST retrieval is 6.61-8.80K, and the RMSE is gradually increased from 3.91 to 5.80 K. This indicates that the LST estimation accuracy gradually decreases with the increase of zenith angle. Therefore, the accuracy of Moon-based LST retrieval algorithm based on microwave remote sensing data depends on the zenith angle.

From the LST derived from the simulated Moon-based microwave radiation brightness temperature data, FY3B MWRI, and AMSR-E brightness temperature data with the same zenith angle, it can be seen that the Moon-based LST retrieval algorithm based on microwave remote sensing data in this study is suitable for different Earth observation platforms. The 23.8 and 36.5 GHz brightness temperatures data are the best for LST retrieval due to the small estimation errors. Moreover, the average error of three LST inversions are 6.78, 6.71, and 6.67K as well as the RMSE are 5.37, 5.18, and 5.44K, respectively, as shown in Fig. 11. Considering the approximate equivalent LST estimation errors using three data with the same viewing zenith angle, the Earth observation platform (Moon-based Earth observation platform, FY3B satellite or Aqua satellite platform) has little effect on the estimation accuracy of Moon-based LST retrieval algorithm using microwave remote sensing data.

The LST estimation error and diurnal temperature variation from FY3B MWRI, AMSR-E, and Moon-based microwave radiation simulation data are given in Table I. Results show that the average error is 6.71, 6.67, and 7.09K and the RMSE is 5.18, 5.44, and 4.79K, respectively. In addition, the diurnal LST variation in the study area is about 60 °C, and the RMSE of the LST inversion result is 3.91–5.80K. This indicates that the estimation error has little effect on the LST relative to the diurnal temperature variation. Therefore, the physical-based retrieval algorithm of Moon-based Earth observation is reliable for the LST estimation using microwave remote sensing data.

In this study, the physical-based retrieval algorithm for LST from Moon-based Earth observation considered in detail the atmospheric effects from the atmospheric transmittance, atmospheric upward and downward radiations. The atmospheric transmittance varies with the changes of the oxygen molecule, water vapor molecule in the atmosphere and the viewing zenith angle, and the accurate results contributes to the high accuracy of the retrieval algorithm. The atmospheric upward and downward radiations was also analyzed in detail instead of being zero or constant in part of the previous studies. Considering the

accurate analysis of these atmospheric parameters, the retrieval accuracy is a little higher than the previous studies. Moreover, the atmosphere and ionosphere parameters are related to the viewing zenith angle, thus the retrieval accuracy changes with the angle. Different Earth observation platforms has a unique viewing zenith angle between 0 and 90°, therefore the retrieval algorithm for LST in this study can be applied to these platforms. The previous studies found that the brightness temperature data of 37 GHz acquired by satellite was optimal for retrieving LST [6]–[8], and the results of this study showed that two frequencies of 23.8 and 36.5 GHz were optimal for Moon-based Earth observation. The estimation accuracy of LST decreased with the decrease of viewing zenith angle. With the viewing zenith angle of larger than 80°, the LST estimation error was up to 5.8K. The phenomenon is related to the low spatial resolution of microwave data, the mixed pixel effect and limitation of the algorithm. Therefore, further research on the reduction of mixed pixel effect, increase of the spatial resolution or improvement of the retrieval algorithm is required.

V. Conclusion

Based on the relationship between horizontal and vertical microwave emissivity in different wavelengths, microwave radiative transfer model and the theory of microwave propagation in the ionosphere, the physical-based retrieval algorithm of LST from passive microwave data for Moon-based Earth observation is developed. The algorithm can simultaneously estimate the LST and the surface emissivity and is applicable to microwave remote sensing data with viewing zenith angle of 0–90°. The key parameters of the algorithm are atmospheric transmittance, atmospheric upward and downward radiations, the attenuation of microwave energy in the ionosphere, and the viewing zenith angle.

After analyzing the atmospheric transmittance, atmospheric upward and downward radiations and the attenuation of microwave energy in the ionosphere for Moon-based Earth observation, it has been observed that the four parameters have a significant correlation with the viewing zenith angle. With the increase of the viewing zenith angle, the atmospheric transmittance decreases gradually from the Moon-based perspective, while the atmospheric upward and downward radiations, and the attenuation of microwave energy increases.

Based on the LST estimation from the FY3B MWRI, AMSR-E, and Moon-based microwave radiation brightness temperature simulation data, the 23.8 and 36.5 GHz brightness temperature data are optimal for the LST estimation under a large-scale viewing zenith angle for Moon-based Earth observation. The average error of LST estimation using the three data are 6.71, 6.67, and 7.09K, and RMSE are 6.17, 5.44, and 4.79K, respectively. Moreover, the RMSE of LST estimation is gradually increasing as the viewing zenith angle increases from 0 to 90°, indicating that the accuracy of LST retrieval increases with the increase of the zenith angle. In addition, the Moon-based LST retrieval algorithm is suitable for passive microwave brightness temperature data from different Earth observation platforms, and the retrieval accuracy is less affected by the platform.

As a part of Moon-based Earth observation research, the study on LST inversion from microwave data can help to clarify the mechanism of microwave radiation energy balance of the Earth's climate system, and provide supports for the Moon-based sensor systems design and the global-scale LST acquisition. In addition, the precision of inversion is usually affected due to the low spatial resolution of microwave data and the mixed pixel effect. To improve the inversion accuracy of the algorithm, further researches on the reduction of mixed pixel effect of different land cover types in certain radiation mechanisms and increase of the spatial resolution will be carried out.

Acknowledgment

The authors would like to thank the National Satellite Meteorological Center of China Meteorological Administration, the National Snow and Ice Data Center (NSIDC), and the National Oceanic and Atmospheric Administration (NOAA) for providing FY3B MWRI data, AMSR-E data, and the USCRN LST data. The authors are also grateful to the International Telecommunication Union Recommendation for providing the P Series P.676-8 recommendation. They would like to thank the anonymous reviewers for their voluntary work and the constructive comments which helped to improve the manuscript.

References

[1] Y. Y. Jia and Z. L. Li, "Progress in land surface temperature retrieval from passive microwave remotely sensed data," *Prog. Geogr.*, vol. 25, no. 3, pp. 96–105, 2006.

[2] G. Maral, J. J. Deridder, B. G. Evans, and M. Richharia, "Low earth orbit satellite systems for communications," *Int. J. Satell. Commun.*, vol. 9, no. 4, pp. 209–225, 1991.

[3] H. D. Guo, G. Liu, Y. X. Ding, Y. L. Zou, S. P. Huang, and L. Jiang, "Moon-based earth observation for large scale geoscience phenomena," in *Proc. IEEE Int. Geosci. Remote Sens. Symp.*, 2016, pp. 546–557.

[4] H. D. Guo, Y. X. Ding, G. Liu, D. W. Zhang, W. X. Fu, and L. Zhang, "Conceptual study of lunar-based SAR for global change monitoring," *Sci. China Earth Sci.*, vol. 57, no. 8, pp. 1771–1779, 2014.

[5] H. D. Guo, "Earth system observation from space: From scientific satellite to Moon-based platform," *J. Remote Sens.*, vol. 20, pp. 716–723, 2016.

[6] M. J. Mcfarland, R. L. Miller, and C. M. Neale, "Land surface temperature derived from the SSM/I passive microwave brightness temperatures," *IEEE Trans. Geosci. Remote Sens.*, vol. 28, no. 5, pp. 839–845, Sep. 1990.

[7] T. R. H. Holmes, R. A. M. De Jeu, M. Owe, and A. J. Dolman, "Land surface temperature from Ka band (37 GHz) passive microwave observations," *J. Geophys. Res.*, vol. 114, no. D4, pp. 0148–0227, 2009.

[8] A. Royer and P. Stéphane, "Surface temperature spatial and temporal variations in North America from homogenized satellite SMMR-SSM/I microwave measurements and reanalysis for 1979–2008," *J. Geophys. Res.*, vol. 115, no. D8, pp. 462–474, 2010.

[9] K. Mao, J. Shi, Z. Li, Z. Qin, M. Li, and B. Xu, "A physics-based statistical algorithm for retrieving land surface temperature from AMSR-E passive microwave data," *Sci. China Ser. D*, vol. 50, no. 7, pp. 1115–1120, 2007.

[10] K. B. Mao, H. J. Tang, L. X. Zhang, M. C. Li, Y. Guo, and D. Z. Zhao, "A method for retrieving soil moisture in Tibet region by utilizing microwave index from TRMM/TMI data," *Int. J. Remote Sens.*, vol. 29, no. 10, pp. 2903–2923, 2008.

[11] L. Gao, R. Fu, R. E. Dickinson, and R. I. Negron Juarez, "A practical method for retrieving land surface temperature from AMSR-E over the amazon forest," *IEEE Trans. Geosci. Remote Sens.*, vol. 46, no. 1, pp. 193–199, Jan. 2008.

[12] A. Basist, N. C. Grody, T. C. Peterson, and C. N. Williams, "Using the special sensor microwave/imager to monitor land surface temperature, wetness, and snow cover," *J. Appl. Meteorol.*, vol. 37, no. 9, pp. 888–911, 1998.

[13] M. Fily, A. Royer, K. Goïta, and C. Prigent, "A simple retrieval method for land surface temperature and fraction of water surface determination from satellite microwave brightness temperatures in sub-arctic areas," *Remote Sens. Environ.*, vol. 83, no. 3, pp. 328–338, 2003.
[14] F. Z. Weng and N. C. Grody, "Physical retrieval of land surface temperature using the special sensor microwave imager," *J. Geophys. Res. Atmos.*, vol. 103, no. D8, pp. 8839–8848, 1998.
[15] L. N. Yuan and J. J. Liao, "Exploring the influence of various factors on microwave radiation image simulation for Moon-based Earth observation," *Front. Earth Sci.*, vol. 13, no. 4, pp. 1–16, 2019, doi: 10.1007/s11707-019-0785-5.
[16] J. A. Otkin, M. C. Anderson, J. R. Mecikalski, and G. R. Diak, "Validation of goes-based insolation estimates using data from the U.S. climate reference network," *J. Hydrometeor.*, vol. 6, no. 4, pp. 460–475, 2005.
[17] K. Goita and A. Royer, "Combination of passive microwave and thermal infrared for the retrieval and analysis of microwave emissivity and temperature," in *Proc. IEEE Int. Geosci. Remote Sens. Symp.*, 2002, pp. 2401–2403.
[18] Z. L. Liu, H. Wu, S. Qiu, Y. Y. Jia, and Z. L. Li, "Determination of land surface temperature from AMSR-E data for bare surfaces," in *Proc. IEEE Int. Geosci. Remote Sens. Symp.*, 2010, pp. 3011–3014.
[19] C. André, C. Ottlé, A. Royer, and F. Maignan, "Land surface temperature retrieval over circumpolar Arctic using SSM/I–SSMIS and MODIS data," *Remote Sens. Environ.*, vol. 162, pp. 1–10, 2015.
[20] K. B. Mao, J. C. Shi, and Z. Li, "Land surface temperature and emissivity retrieved from AMSR passive micro-wave data," in *Proc. IEEE Int. Geosci. Remote Sens. Symp.*, 2005, pp. 2247–2249.
[21] S. Chen, X. Chen, W. Chen, Y. Su, and D. Li, "A simple retrieval method of land surface temperature from AMSR-E passive microwave data—A case study over Southern China during the strong snow disaster of 2008," *Int. J. Appl. Earth Observ.*, vol. 13, no. 1, pp. 140–151, 2011.
[22] Y. B. Qiu, L. J. Shi, J. C. Shi, and S. J. Zhao, "Atmospheric influences analysis on the satellite passive microwave remote sensing," *Spectrosc. Spectral Anal.*, vol. 36, no. 2, pp. 310–315, 2016.
[23] J. A. Sobrino, Z. L. Li, and M. P. Stoll, "Impact of the atmospheric transmittance and total water vapor content in the algorithms for estimating satellite sea surface temperatures," *IEEE Trans. Geosci. Remote Sens.*, vol. 31, no. 5, pp. 946–952, Sep. 1993.
[24] A. S. Joshi and G. N. Tiwari, "Evaluation of solar radiation and its application for photovoltaic/thermal air collector for Indian composite climate," *Int. J. Energy Res.*, vol. 31, no. 8, pp. 811–828, 2007.
[25] International telecommunication union recommendation P.676-11. [Online]. Available: https://www.itu.int/rec/R-REC-P.676-8-200910-S/en. Accessed on: Mar. 3, 2010.
[26] H. E. Fleming, D. S. Grosby, and A. C. Neuendorffer, "Correction of satellite temperature retrieval errors due to errors in atmospheric transmittances," *J. Climate Appl. Meteor.*, vol. 25, no. 6, pp. 869–882, 1986.
[27] L. M. McMillin, X. Xiong, Y. Han, T. J. Kleespies, and P. Van Delst, "Atmospheric transmittance of an absorbing gas. 7. Further improvements to the OPTRAN 6 approach," *Appl. Opt.*, vol. 45, no. 9, pp. 2028–2034, 2006.
[28] J. A. Sobrino, Z. L. Li, and M. P. Stoll, "Impact of the atmospheric transmittance and total water vapor content in the algorithms for estimating satellite sea surface temperatures," *IEEE Trans. Geosci. Remote Sens.*, vol. 31, no. 5, pp. 946–952, Sep. 1993.
[29] S. E. Hannon, L. L. Strow, and W. W. Mcmillan, "Atmospheric infrared fast transmittance models: A comparison of two approaches," *Proc. SPIE*, pp. 94–105, 1996.
[30] S. A. Clough, F. X. Kneizys, and L. S. Rothman, "Atmospheric spectral transmittance and radiance - FASCOD1B," *Proc. SPIE*, vol. 277, no. 12, pp. 152–166, 1980.
[31] B. K. Kristina, A. M. Lynn, and J. L. Richard, "Albedo of a water surface, spectral variation, effects of atmospheric transmittance, sun angle and wind speed," *J. Geophys. Res. Oceans.*, vol. 90, no. C4, pp. 7313–7321, 1985.
[32] N. Nijegorodov, K. R. S. Devan, and P. K. Jain, "Atmospheric transmittance models and an analytical method to predict the optimum slope of an absorber plate, variously oriented at any latitude," *Renewable Energy*, vol. 4, no. 5, pp. 529–543, 1994.
[33] T. T. Shu, "Using of temperature weighting functions for retrieving atmospheric temperature profiles of the relevant theoretical research," *J. Microw.*, vol. 8, pp. 51–454, 2012.
[34] D. N. Feng, "Retrieval and validation of land surface temperature from AMSR2 data," M.S. Thesis, School Resources Envir., Univ. Electron. Sci. Technol. China, Sichuan, China, 2016.
[35] K. C. Wang and S. L. Liang, "Global atmospheric downward longwave radiation over land surface under all-sky conditions from 1973 to 2008," *J. Geophys. Res. Atmos.*, vol. 114, no. D19101, pp. 1–12, 2009.
[36] A. Masaru and Y. Masataka, "Observations of atmospheric downward radiation in the Tokyo area," *Boundary Layer Meteorol.*, vol. 16, no. 4, pp. 453–465, 1979.
[37] G. Abramowitz, L. Pouyanné, and H. Ajami, "On the information content of surface meteorology for downward atmospheric long-wave radiation synthesis," *Geophys. Res. Lett.*, vol. 39, no. 4, 2012, Art. no. L04808.
[38] E. Barbaro *et al.*, "Observational characterization of the downward atmospheric longwave radiation at the surface in the city of São Paulo," *J. Appl. Meteor. Climatol.*, vol. 49, no. 12, pp. 2574–2590, 2010.
[39] M. F. Huang, X. F. Xing, and S. H. Liu, "Estimation of downward atmospheric long-wave radiation using thermal inertia based on remote sensing," *Resour. Sci.*, vol. 28, no. 3, pp. 37–43, 2006.
[40] M. F. Huang, J. Q. Li, and X. F. Wang, "Retrieving downward atmospheric long-wave radiation using satellite data," in *Proc. IEEE Int. Geosci. Remote Sens. Symp.*, 2008, pp. 4390–4393.
[41] K. Wang and R. E. Dickinson, "Global atmospheric downward longwave radiation at the surface from ground-based observations, satellite retrievals, and reanalyses," *Rev. Geophys.*, vol. 51, no. 2, pp. 150–185, 2013.
[42] E. I. Nezval, N. E. Chubarova, J. Gröbner, and A. Omura, "Influence of atmospheric parameters on downward longwave radiation and features of its regime in Moscow," *Izv. Atmos. Ocean. Phys.*, vol. 48, no. 6, pp. 610–617, 2012.
[43] M. Laroussi and J. R. Roth, "Numerical calculation of the reflection, absorption, and transmission of microwaves by a nonuniform plasma slab," *IEEE T. Plasma Sci.*, vol. 21, no. 4, pp. 366–372, 1993.
[44] W. X. Cai, "Research on propagation characteristics of radio waves in heating ionosphere," M.S. Thesis, School Phys. Optoelectron. Eng., Xidian Univ., Xian, China, 2015.
[45] M. Indira Devi, I. Khan, and D. N. M. Rao, "A study of VLF wave propagation characteristics in the Earth-ionosphere waveguide," *Earth Planets Space*, vol. 60, no. 7, pp. 737–741, 2008.
[46] F. He, "Ionospheric loss of high frequency radio wave propagated in the ionospheric regions," *J. Radio Sci.*, vol. 24, pp. 720–723, 2009.
[47] R. S. Lawrence, C. G. Little, and H. J. A. Chivers, "A survey of ionospheric effects upon earth-space radio propagation," *Proc. IEEE*, vol. 52, no. 1, pp. 4–27, Jan. 1964.
[48] W. Zou, D. T. Hou, Q. Wang, Z. X. Niu, and D. F. Zhou, "Refractive index of HPM at transionospheric propagation," *High Power Laser Part. Beams*, vol. 18, no. 10, pp. 1673–1676, 2006.
[49] C. J. Gibbins, C. L. Wrench, and D. L. Croom, "Clear sky atmospheric emission measurements at frequencies of 22, 95, 110, 123, and 150 GHz," *Int. J. Infrared Millimeter Waves*, vol. 5, no. 11, pp. 1443–1472, 1984.

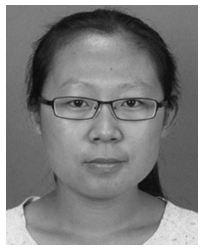

Linan Yuan received the Graduate degree in surveying and mapping engineering from the China University of Mining & Technology, Beijing, China, in 2016. Since September 2016, she has been working toward the Ph.D. degree with the Department of Geographical Information System, Aerospace Information Research Institute, Chinese Academy of Sciences, Beijing, China, and the University of Chinese Academy of Sciences, Beijing, China. Her current research activities deal with the moon-based earth observation.

Jingjuan Liao received the B.S. and M.S. degrees in geoscience from Nanjing University, Jiangsu, China, in 1987 and 1990, respectively, and the Ph.D. degree in geophysics from the Institute of Geophysics, Chinese Academy of Sciences, Beijing, China, in 1993.

Since 1993, she has been working on radar remote-sensing applications as a Researcher with the Institute of Remote Sensing Applications, Chinese Academy of Sciences. Since 2007, she has been working on microwave remote-sensing application as a Professor with the Center for Earth Observation and Digital Earth and the Institute of Remote Sensing and Digital Earth, Chinese Academy of Sciences. She is currently working at the Key Laboratory of Digital Earth Science, Aerospace Information Research Institute, Chinese Academy of Sciences. She has completed several research projects, and published more than 90 paper in relevant journals. Her current research interests include microwave scattering model, data processing, and surface parameters estimation.